

1 **Regional Features of the 20-30 Day Periodic Behavior**  
2 **in the Southern Hemisphere Summer Circulation**

3 **Zhaoyu Liu<sup>1</sup>, Lei Wang<sup>1</sup>**

4 <sup>1</sup>Department of Earth, Atmospheric, and Planetary Sciences, Purdue University

5 **Key Points:**

- 6 • The hemispheric 20-30 day periodicity in the austral summer has a strong local-  
7 ization in local wave activity and precipitation.  
8 • Strong enhancement of intraseasonal variability and local periodic behavior is iden-  
9 tified within the South Pacific.  
10 • The local nature of 20-30 day periodicity offers a potential source of intraseasonal  
11 predictability for weather analysts and forecasters.

---

Corresponding author: Lei Wang, [leiwang@purdue.edu](mailto:leiwang@purdue.edu)

12 **Abstract**

13 The Southern Hemispheric (SH) storm tracks exhibit a robust intraseasonal peri-  
 14 odicity of 20-30 days as the leading mode of zonal-mean eddy kinetic energy. To what  
 15 extent this hemispheric-scale mode of variability translates to smaller scales remains de-  
 16 bated. This work studies the regional features of SH storm tracks through the filtered  
 17 variance of local finite-amplitude wave activity. While the synoptic variance is zonally  
 18 elongated over the storm track, we find a strong enhancement of intraseasonal variabil-  
 19 ity within the South Pacific with a minimum strength of the storm track. This enhanced  
 20 region is marked with 20-30 day periodic behavior of local wave activity and precipita-  
 21 tion and is driven by enhanced variability of low-level eddy heat flux on the same timescale.  
 22 The local nature of 20-30 day periodicity offers a potential source of intraseasonal pre-  
 23 dictability for weather analysts and forecasters.

24 **Plain Language Summary**

25 Storm activities in Southern Hemisphere (SH) midlatitudes are characterized by  
 26 20-30 day periodic behavior, representing a hemispheric-scale pulsing of zonal-mean ex-  
 27 tratropical eddy activity. This phenomenon has been termed the Baroclinic Annular Mode  
 28 (BAM) defined as the leading EOF mode of the zonal-mean eddy kinetic energy. If this  
 29 large-scale mode were to have a strong local nature, such periodic behavior in subseasonal-  
 30 to-seasonal time scale would have important implications for understanding and predict-  
 31 ing the medium-range weather system, especially for extreme events. However, to what  
 32 extent we can identify regional features of such hemispheric-scale mode of variability re-  
 33 mains unclear.

34 We demonstrate the regional feature of this periodic variability by showing the vari-  
 35 ance of local wave activity in different time scales. We find that the variability in a shorter  
 36 weather time scale (2-7 days) exhibits a largely zonally-symmetric structure, but the vari-  
 37 ability in the intraseasonal time scale exhibits a strong localization concentrated in the  
 38 South Pacific. We further assess the distribution of periodicity within the intraseasonal  
 39 variability and find that the 20-30 day periodicity is also localized within South Pacific.  
 40 The local nature of this 20-30 day periodicity indicates the potential utility of the BAM  
 41 for weather analysts and forecasters.

42 **1 Introduction**

43 High-quality societal applications for decision-makers for optimizing resource man-  
 44 agement and preventing disaster require accurate sub-seasonal to seasonal (S2S, intrasea-  
 45 sonal) predictions, because high-impact extreme weather events, such as long-lasting heat-  
 46 waves and extreme cold spells, often occur on this timescale. Recent research has iden-  
 47 tified multiple sources of S2S predictability, such as the Madden-Julian oscillation (MJO),  
 48 the basic state of the ENSO, soil moisture, tropical-extratropical teleconnections, etc (see  
 49 the review in (Vitart et al., 2017)). However, nearly all of these sources are outside of  
 50 the midlatitude internal dynamics. This is due to the conventional understanding that  
 51 the large-scale midlatitude variability is typically consistent with Gaussian red noise rather  
 52 than periodic behaviors (Feldstein, 2000; Lorenz & Hartmann, 2001). As a 'null hypoth-  
 53 esis,' intraseasonal variability can be considered as a response to stochastic forcing by  
 54 higher-frequency synoptic system's disturbances (Leith, 1973; Hasselmann, 1976; Green,  
 55 1977). Assuming synoptic disturbances as Gaussian white noise forcing  $F_t$ , this 'null hy-  
 56 pothesis' suggests the time series of intraseasonal variability  $x_t$  as a Gaussian red noise  
 57 process  $x_t = \alpha x_{t-1} + F_t$ , where  $\alpha$  is a positive constant defining the e-folding timescale  
 58 of the intraseasonal variability. Hence, no unique source of predictability on regional scales  
 59 has been identified within the midlatitude atmosphere beyond the synoptic weather range.

60 Baroclinic Annular Mode (BAM), however, a recently discovered large-scale mid-  
61 latitude variability over the SH, is characterized by a robust intraseasonal periodicity about  
62 20-30 day (Thompson & Barnes, 2014; Thompson & Woodworth, 2014). BAM is defined  
63 by the leading empirical orthogonal function (EOF) of the zonal-mean eddy kinetic en-  
64 ergy (EKE), representing the intraseasonal oscillation of eddy activity on a hemispheric  
65 scale. If such periodic nature were to translate to smaller scales at certain regions, it could  
66 serve as a new source of S2S predictability. In a regional scale study of BAM, Thompson  
67 et al. (2017) find that the periodicity in the upper troposphere eddy kinetic energy is not  
68 apparent at a fixed location. As the averaging windows reduce from the entire global circle  
69 to 30-degree wide regions, the power spectra reduce from a robust quasi-periodic shape  
70 to a red noise without any major enhancement of the variance on the 20-30 day frequency  
71 range. The discovery of the lack of local periodicity for regions smaller than 30 degrees  
72 is explained through a conceptual model featuring out-of-phase anomalies between the  
73 upper and lower troposphere. A similar finding was also confirmed in Xue et al. (2021),  
74 that the domain should be wide enough to accommodate a wave packet so that the in-  
75 traseasonal periodicity can be identified. Therefore, as the averaging domain size reduces  
76 to smaller scales, periodic behavior at a fixed region is not expected, which is consistent  
77 with the above 'null hypothesis.' To what extent such a leading mode of variability is  
78 translated to regional scale intraseasonal variability - and thus modulating serial clus-  
79 tering of extreme weather events - remains an open question.

80 To address this question, we will adopt a filtered variance approach, which has been  
81 well-developed to identify the geographic distributions of the storm tracks (Blackmon  
82 et al., 1977). Typically, a scalar quantity combining multiple information is preferred,  
83 such as the 500 hPa geopotential height field (Z500), which is related to both the wind  
84 and temperature. Blackmon et al. (1977) developed this filtered variance framework us-  
85 ing the Northern Hemisphere (NH) Z500, with the spectral domains separated into syn-  
86 optical and intraseasonal bands, respectively (also see Blackmon et al. (1984)). Through  
87 a similar filtered variance analysis, Trenberth (1981, 1991) studied the SH circulation  
88 within synoptic time scales and found that the SH storm tracks exhibit strong zonal sym-  
89 metry along with a maximum located at the Southern Indian Ocean and a minimum at  
90 the South Pacific. Kidson (1991) found a zonal-symmetric pattern for the intraseasonal  
91 variability in the SH (see also Hartmann (2015)). Therefore, we aim to make progress  
92 on deepening the understanding of the regional features of the intraseasonal variability  
93 - a less explored territory. Specifically, we ask: are these regions with enhanced intrasea-  
94 sonal variance mainly characterized by a Gaussian red-noise spectrum as expected from  
95 the 'null hypothesis,' or have certain quasi-periodic behaviors that may be connected with  
96 the hemispheric-scale 20-30 day periodic mode of variability?

97 To answer this question, we start with the surface precipitation analysis, a directly  
98 measured quantity as a surrogate for the local behavior of storm activities. Then we will  
99 quantify the regional variability pattern by applying the filtered variance approach (Blackmon  
100 et al., 1977) to key representative variables, including Z500, EKE, and a newly devel-  
101 oped quantity local wave activity (LWA), as well as the low-level eddy heat flux that drives  
102 LWA tendency. This work focuses on Austral summer season (DJF) since the periodic  
103 behavior is much more significant in austral summer than other seasons (Wang & Naka-  
104 mura, 2015). Comparisons to the Northern Hemisphere and with different seasons will  
105 be addressed in follow-up studies. The paper is organized as follows. In Section 2, we  
106 introduce data and key methodologies such as LWA and filtered variance framework. In  
107 Section 3, we first discuss the regional features of surface precipitation and then demon-  
108 strate the synoptic and intraseasonal variability patterns of different variables associated  
109 with spectral analysis. Section 4 concludes with a summary.

## 2 Data and Method

We use ECMWF-Interim reanalysis products, including zonal and meridional velocities, air temperature, and geopotential height, with a horizontal resolution  $1.25^\circ \times 1.25^\circ$  and daily resolution from 1979 to 2018. Additionally, the daily precipitation is obtained from the Advanced Microwave Scanning Radiometer (AMSR) -E from 2003 to 2010 processed by a three-day moving average. AMSR-E measures the surface rain rate covering from  $70^\circ\text{N}$ - $70^\circ\text{S}$ .

The filtered variability approach is based on the standard deviation in the 2-7 day band for synoptic analysis and the 10-45 day band for intraseasonal analysis. The temporal filter is based on Fast Fourier Transform (FFT) with Hanning window from 1 December to 28 February between 1979 and 2018. The framework is applied to Z500, EKE, LWA, and 850hPa eddy heat flux, respectively. EKE is defined as  $((u^*)^2 + (v^*)^2)/2$  and is averaged with density weighting along the vertical column. 850hPa eddy heat flux is defined as  $v^*T^*$ , where the asterisks represent the departures from the zonal mean.

Unlike EKE, local finite-amplitude wave activity emphasizes on coherent meandering of the contours of a quasi-conserved quantity. Conserving flow circulation through Kelvin's circulation theorem, the area bounded by the reference quantity contour is the same as the one bounded by the latitude circle. Finite-amplitude wave activity (FAWA, see N. Nakamura and Zhu (2010)) focuses on the total displacement over the entire longitudes, while LWA (see Huang and Nakamura (2016), Chen et al. (2015)) measures the displacement for each longitude, so that a full longitude-latitude pattern of wave activity can be quantified. For example, the field of Z500 can be used to define the local wave activity (Chen et al., 2015):

$$A_{z500}(\phi_e, \lambda, t) = \frac{a}{\cos\phi_e} \left( \int_{z' \geq 0, \phi \leq \phi_e, \lambda = \text{const}} z' \cos\phi d\phi - \int_{z' \leq 0, \phi \geq \phi_e, \lambda = \text{const}} z' \cos\phi d\phi \right), \quad (1)$$

where  $a$  is the earth radius,  $\phi$ ,  $\lambda$ , represents the latitude and longitude respectively,  $z' = z - Z(\phi_e)$  is the deviation from the reference Z500 contour  $Z(\phi_e)$  at its equivalent latitude  $\phi_e$ . The relation between  $Z(\phi_e)$  and  $\phi_e$  is connected by the same bounded area  $\phi_e(Z) = \arcsin[1 - \frac{S(Z)}{2\pi a^2}]$ .

A quasi-geostrophic potential vorticity (QGVPV) -based LWA allows one to quantify the role of eddy forcing. Local wave activity at each pseudo-height level can be assessed independently, and the density-weighted vertically averaged value is used to represent the barotropic wave activity. See supplementary material for more details.

## 3 Results

We start with analyzing the temporal and spatial features of precipitation, since surface rain rate is a directly measured quantity by space-based meteorological satellites, and is highly correlated with the variability of storm activity. Thompson and Barnes (2014) found that the mid-latitude mean precipitation can also exhibit a significant intraseasonal periodicity around 20-30 days as a key feature of BAM. Is there any localization of such periodic behavior in the precipitation?

To illustrate the regional feature, we calculated the power spectra of surface rain rate retrieved from AMSR-E in four separated regions as shown in Figure 1c:  $0^\circ$ - $90^\circ\text{E}$ ,  $90^\circ\text{E}$ - $180^\circ$ ,  $180^\circ$ - $90^\circ\text{W}$ ,  $90^\circ\text{W}$ - $0^\circ$ , all of which are averaged between  $40^\circ\text{S}$ - $50^\circ\text{S}$ , and we find that the most significant 20-30 day periodicity is located at the South Pacific ( $180^\circ$ - $90^\circ\text{W}$  with 95% confidence level), while spectra features in other three regions are mainly characterized by enhanced synoptic variability ( $0^\circ$ - $180^\circ\text{E}$ ) or similar to a red-noise ( $90^\circ\text{W}$ - $0^\circ$ ). Thus, there is a localization of the surface rain rate's 20-30 day periodic behavior. Is this localization of rain rate periodicity a coincidence? Or it implies a strong local-

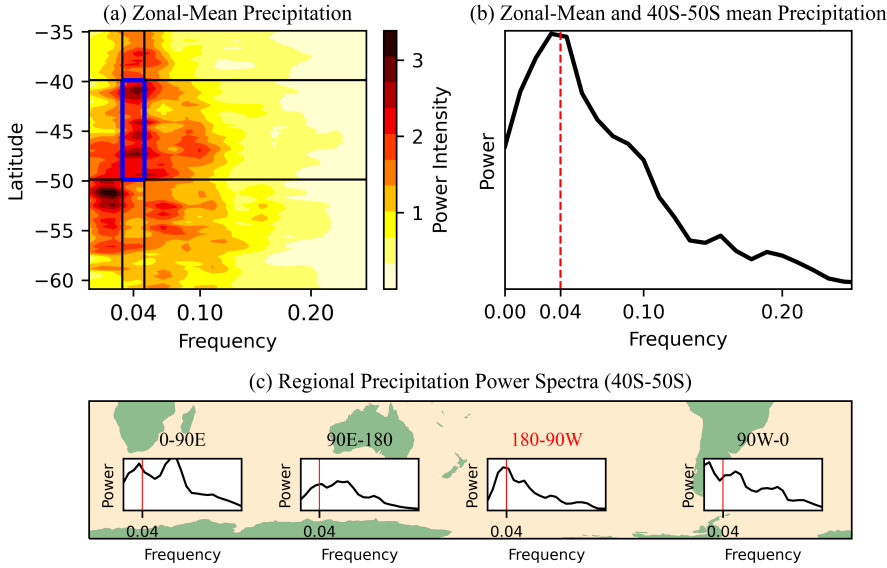


Figure 1: Power spectra of surface precipitation in austral summer (DJF) from 2002-2010 for (a) zonal-mean, (b) zonal-mean and averaged between 40°S-50°S, (c) regional mean of 0°-90°E, 90°E-180°, 180°-90°W, 90°W-0°, all of which averaged between 40°S-50°S.

147 ization of the 20-30 day periodic behavior for the underlying large-scale atmospheric cir-  
 148 culation?

149 We adopt the filtered variance approach of Blackmon et al. (1977) to quantify the  
 150 regional features of synoptic and intraseasonal variability, respectively. The variability  
 151 of Z500 exhibits a more zonally symmetric regional pattern within both synoptic and  
 152 intraseasonal timescales as consistent with the previous work (see Supplementary Fig-  
 153 ure S1). Centered around 50°S, the synoptic variance is strongest in the South Indian  
 154 Ocean, while the maximum of intraseasonal variance is zonally elongated over much of  
 155 the South Pacific. The zonal-mean Z500 field does not show any periodic behavior in the  
 156 intraseasonal timescales (see Supplementary Figure S2), thus we would not expect any  
 157 local periodic behavior in the Z500 field.

158 As the variable central to the BAM definition, zonal-mean EKE is characterized  
 159 by a robust periodic behavior (Thompson & Woodworth, 2014). However, as Thompson  
 160 et al. (2017) discovered, the periodicity in EKE is not apparent at a fixed location, and  
 161 we find consistent results that the regional variability is much weaker in the intrasea-  
 162 sonal band at pixel (i.e., grid point) level (see Supplementary Figure S3). Instead, a two-  
 163 branch structure is observed in the intraseasonal variance pattern of EKE, and can be  
 164 attributed to the intense wave-breaking processes at the South Pacific that generate in-  
 165 tense local values of zonal and meridional velocities, since qualitatively speaking, EKE  
 166 reaches maximum where the circulation contours are the densest. The two-branch struc-  
 167 ture belongs to the same storm activity region - as the below LWA analysis would illus-  
 168 trate more clearly.

169 Therefore, an accurate diagnostic approach for eddy activity that can illustrate both  
 170 spatial and temporal features is required to study our key question. As a comparison with  
 171 Z500 or EKE, the local finite-amplitude wave activity (LWA) provides a more objective

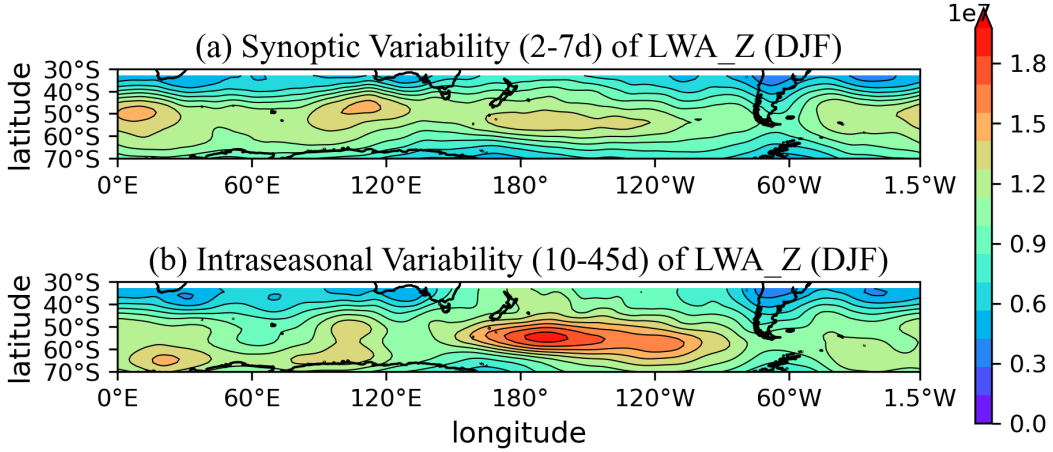


Figure 2: Bandpass-filtered variance converted to standard deviation for Z500-based LWA (LWA\_Z) in austral summer(DJF): (a)synoptic variability(2-7 days), and (b)intraseasonal variability(10-45 days). The shading represents values between  $0m^2$  and  $1.9 \times 10^7m^2$ .

172 approach for the diagnostic of eddy activity. QGPV-based LWA is a conserved quantity  
 173 and driven by eddy flux terms - each bearing clear physical interpretations, directly rep-  
 174 resenting the pseudo-momentum carried by eddy. Z500-based LWA shares many features  
 175 of the QGPV-based LWA, and it is more straightforward to calculate. Regarding the spa-  
 176 tial feature, LWA can capture the breaking waves as part of an underlying coherent pat-  
 177 tern (see the comparison between LWA and EKE in Huang and Nakamura (2017)). For  
 178 example, for a large-scale dipole structure, the maximum value of LWA locates only at  
 179 the center of the overturning contours of PV (or Z500). In contrast, the maximum val-  
 180 ues of EKE are found at two distinct places - the edge of the upper high-pressure sys-  
 181 tem and the edge of the lower low-pressure system. Regarding the temporal feature, Wang  
 182 and Nakamura (2015) confirmed that FAWA also exhibits a robust 20-30 day periodic-  
 183 ity, consistent with features of BAM defined by the EOF-based EKE framework. Since  
 184 zonal-average of LWA naturally conforms to FAWA, LWA has the strength to pinpoint  
 185 regional features more precisely, and to allow for a direct connection with the hemispheric-  
 186 scale 20-30 day periodic behavior as defined by FAWA. Both the QGPV and Z500 fields  
 187 can be used to calculate the LWA, with the former directly connected with the eddy fluxes  
 188 terms and the latter more commonly available among climate model outputs. Our anal-  
 189 ysis confirms that both approaches yield qualitatively consistent results.

190 Figure 2 shows the synoptic and intraseasonal variability pattern of Z500-based LWA  
 191 in austral summer. The synoptic variability still exhibits a zonally symmetric pattern,  
 192 with the maximum variance concentrated in the Southeast (SE) Indian Ocean as well  
 193 as in the SE Atlantic, and the minimum variance in the SE Pacific close to South Amer-  
 194 ica (also see Supplementary Figure S4 for QGPV-based LWA). This result is qualitatively  
 195 consistent with the pattern shown by the filtered variance of the Z500 field, but further  
 196 captures a more detailed and coherent structure clearly emphasizing the maximum re-  
 197 gion. Such intensified synoptic variability at the SE Indian Ocean and Atlantic can be  
 198 largely attributed to the downstream development of baroclinic waves (Berbery & Vera,  
 199 1996), and therefore the largest synoptic variance is expected to occur closely downstream  
 200 to the regions of maximum observed baroclinicity, which is located at the Southwest (SW)  
 201 Indian Ocean and SW Atlantic (the sea surface temperature frontal zones, see H. Naka-

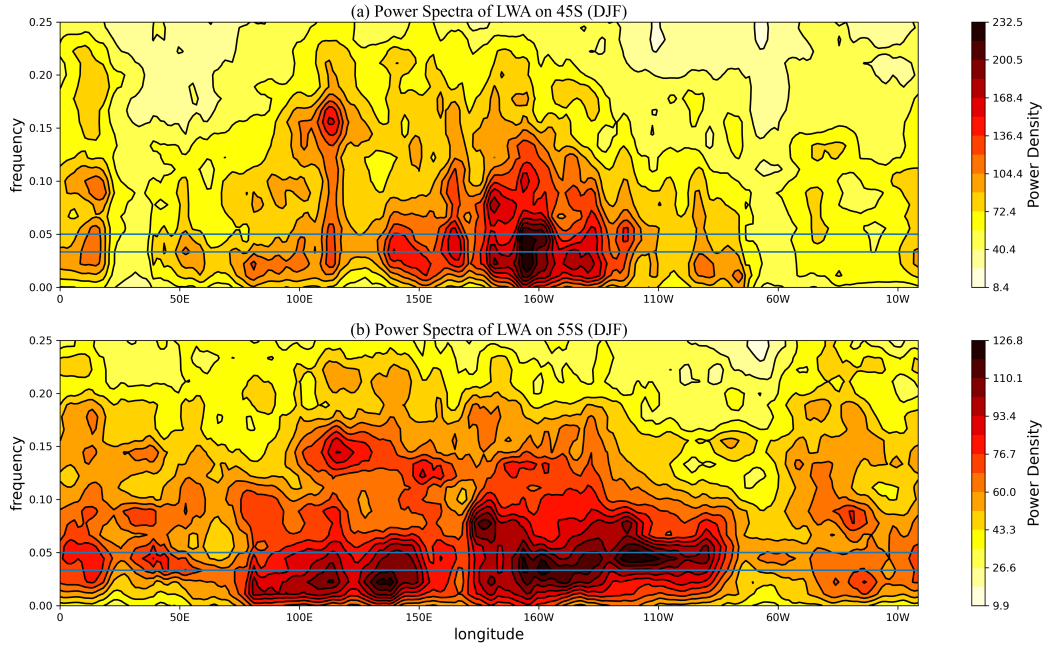


Figure 3: Power spectra of QGPV-based LWA as functions of longitude and frequency at two representative latitudes 45°S (upper panel) and 55°S (lower panel), respectively.

202 mura and Shimpo (2004)). The weakened synoptic signal at the South Pacific is asso-  
 203 ciated with the decaying process of extratropical cyclones' lifecycles.

204 With an ability to capture larger-scale meandering, the filtered variance of Z500-  
 205 based LWA captures the corresponding intraseasonal variability more efficiently than that  
 206 of the Z500 and EKE field. As shown in Figure 2b, the intraseasonal variance of LWA  
 207 is near twice its synoptic counterpart. Besides, the intraseasonal pattern is not as zonally-  
 208 elongated as the synoptic variance or the pattern captured by Z500. In contrast, a strong  
 209 local enhancement is found confined at the South Pacific, largely within 180°-150°W and  
 210 50°S-60°S. This region is right at the center between the two branches shown in the in-  
 211 traseasonal pattern of EKE (Supplementary Figure S3b), which demonstrates the ad-  
 212 vantage of LWA in capturing coherent patterns for large-scale eddies. Similarly, the fil-  
 213 tered variance of QGPV-based LWA shows consistent results: a robust intensification  
 214 of intraseasonal variability at the South Pacific is observed located within 180°-150°W  
 215 (see Supplementary Figure S4b). Despite the minor difference that the QGPV-based LWA  
 216 shows a more equatorward intraseasonal pattern, both types of the filtered variance of  
 217 LWA show a consistent key region of intraseasonal variability of storm activities confined  
 218 within the South Pacific.

219 With a region of enhanced intraseasonal variance pinned down, we next investigate  
 220 whether the enhanced frequencies is related to the 20-30 day periodic mode. To zoom  
 221 into the crucial latitudes where such periodicity is concentrated. Figure 3 shows the power  
 222 spectra of QGPV-based LWA as the function of longitudes and frequencies at 45°S and  
 223 55°S, since Wang and Nakamura (2015) found that the 20-30 day periodic variability mainly  
 224 dominates the midlatitudes from 40°S-60°S (also see Supplementary Figure S5). Within  
 225 the intraseasonal domain, the 20-30 day periodicity (0.03-0.05 cpd, bounded by two blue

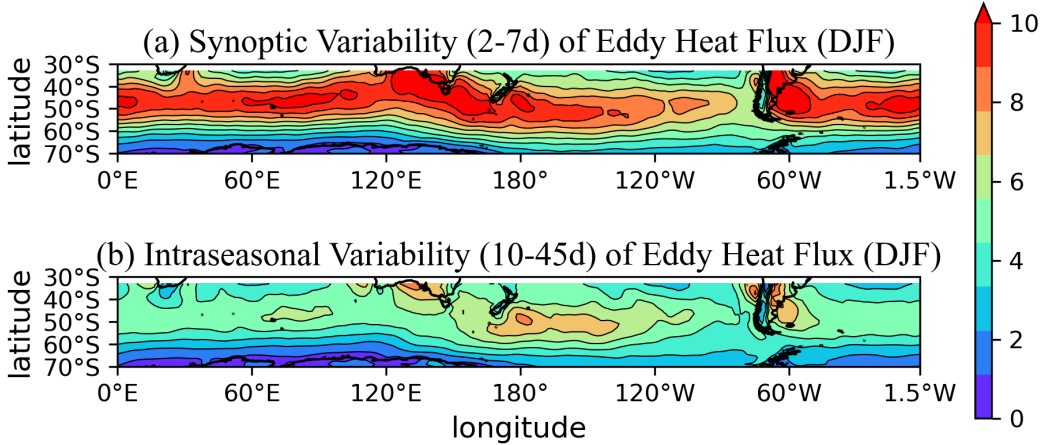


Figure 4: Bandpass-filtered variance converted to standard deviation for 850hPa eddy heat flux in austral summer(DJF): (a)synoptic variability(2-7 days), and (b)intraseasonal variability(10-45 days). The shading represents values between  $0mK/s$  and  $10mK/s$ .

lines in Figure 3) exhibits a strong localization as hinted by the filtered variance approach. At 45°S for example, the strongest 20-30 day frequency band is largely confined between 180°-150°W, overlapping the region where the intraseasonal variance reaches its maximum (shown in Figure 2b). This regional feature of periodicity might slightly vary with different latitudes, for example the most significant 20-30 day periodicity at 55°S exhibits an elongated range covering 180°-100°W. By and large, all cross sections within mid-latitudes demonstrate that the 20-30 day periodicity has a strong regional preference located at the South Pacific. A similar result can be observed if the LWA is meridionally averaged between 40°S-60°S (see Supplementary Figure S6), the 20-30 day periodicity is still strongly localized at the South Pacific, resembling the pattern at individual latitudes. Note that, in this case, the budget term of meridional eddy momentum flux is removed due to the meridional average, and therefore it can suggest that, the meridional eddy momentum flux plays a non-dominant role in the intraseasonal variability. The zonal wave flux convergence, as another important budget term of LWA, will not directly impact LWA's intraseasonal variability neither, as the zonal wave flux convergence primarily populate the synoptic variability of wave activity (Huang & Nakamura, 2017). The cross-section of power spectra for Z500-based LWA shows similar results to the QGPV-based LWA, whereas that for EKE does not show robust 20-30 day periodicity (see Supplementary Figure S7 and S8).

What would be a key factor that drives such locally confined intraseasonal variability including the 20-30 day periodicity? Wang and Nakamura (2015, 2016) find that eddy forcing due to the low-level eddy heat flux drives the 20-30 day periodicity in zonal-mean of LWA (i.e., FAWA). A local enhanced variance of eddy heat flux should be expected if this can also translate into regional scales. Figure 4 confirmed this expectation by showing that the intraseasonal variance of 850hPa eddy heat flux is also localized between 180°-150°W, largely overlapping the region where the intraseasonal variance of LWA is strongly enhanced, as shown in Figures 2 and 3. The cross-section power spectra of 850 hPa eddy heat flux further indicates that the low-level eddy heat flux also exhibits enhanced 20-30 day periodicity at fixed locations, largely confined within the South Pacific as well (see Supplementary Figure S9). This locally enhanced intraseasonal variability of 850hPa eddy heat flux is marked with a strong r.m.s. eddy streamfunction as a surrogate of eddy diffusivity for estimating the horizontal eddy heat flux (Kushner &

258 Held, 1998; Held, 1999). Strong thermal damping over this area reduces linear baroclinic  
259 eddy growth rates (Swanson & Pierrehumbert, 1997). Thus, this sufficient temperature  
260 homogenization in the lower troposphere sustains states neutral to the growth of syn-  
261 optic eddies but favorable to intraseasonal variability and the associated periodic behav-  
262 ior.

## 263 4 Conclusion and Discussion

264 We study the regional features of storm tracks' 20-30 day periodic variability in aus-  
265 tral summer by applying the filtered variance approach to local wave activity. While the  
266 synoptic variance is largely zonally elongated over the storm track, we find a strong lo-  
267 cal enhancement of intraseasonal variability within the South Pacific with a minimum  
268 strength of the storm track. For this region, we find that this enhanced region is marked  
269 with local 20-30 day periodic behavior of precipitation and local wave activity whereby  
270 rejecting the 'null hypothesis' that intraseasonal variability is nothing more than a red-  
271 noise response to stochastic forcing by synoptic transients. The local periodicity is driven  
272 by enhanced variability of low-level eddy heat flux on the same timescale. The filtered  
273 variance of LWA analysis offers insights into the regional features of the coherent and  
274 slowly meandering structures of the circulation.

275 Internal modes of variability, such as BAM, result from the deterministic dynam-  
276 ics of the atmosphere. Thus a translation into regional scales may indicate unique pre-  
277 dictability beyond the typical weather range. While the fundamental dynamics of BAM  
278 remain an open question, it is clear that cross-scale interactions between the synoptic  
279 and intraseasonal scales set the regional structure of this internal mode. The local na-  
280 ture of the 20-30 day periodicity identified by local wave activity provides a potential  
281 source of intraseasonal predictability for weather analysts and forecasters. As an inter-  
282 nal mode that has yet to be tapped for extending the forecast beyond the typical weather  
283 range, more work is needed to connect this intraseasonal mode of variability with serial  
284 clustering of extreme weather events to quantify this potential regional predictability.  
285 In a warming climate, BAM is projected to increase its strength (Wang et al., 2018). A  
286 further implication of this work is the question of how the intraseasonal mode of vari-  
287 ability and the associated regional impacts will evolve as climate changes. With the rapid  
288 development of high-resolution Earth system modeling, we are at a crucial era to deepen  
289 our understanding of the synoptic-intraseasonal interactions and the associated Earth  
290 system's regional variability and predictability.

## 291 5 Data Availability Statement

292 The authors acknowledge the use of NASA AMSR-E product for precipitation dataset:  
293 <https://www.earthdata.nasa.gov/sensors/amsr-e>, and ERA-Interim reanalysis dataset:  
294 <https://apps.ecmwf.int/datasets/data/interim-full-daily/>. The open reposi-  
295 tory including codes and related data for plotting key figures in this work is pasted here:  
296 <https://doi.org/10.5281/zenodo.7855573>

## 297 Acknowledgments

298 The authors acknowledge to NASA for providing AMSR-E precipitation observation and  
299 ECMWF for providing ERA-Interim reanalysis dataset.

## 300 References

301 Berbery, E. H., & Vera, C. S. (1996, February). Characteristics of the South-  
302 ern Hemisphere Winter Storm Track with Filtered and Unfiltered Data.  
303 *Journal of the Atmospheric Sciences*, 53(3), 468–481. Retrieved 2023-04-

- 304 16, from [https://journals.ametsoc.org/view/journals/atsc/53/3/](https://journals.ametsoc.org/view/journals/atsc/53/3/1520-0469_1996_053_0468_cotshw_2_0_co_2.xml)  
 305 1520-0469\_1996\_053\_0468\_cotshw\_2\_0\_co\_2.xml (Publisher: American  
 306 Meteorological Society Section: Journal of the Atmospheric Sciences) doi:  
 307 10.1175/1520-0469(1996)053<0468:COTSHW>2.0.CO;2
- 308 Blackmon, M. L., Lee, Y.-H., & Wallace, J. M. (1984, March). Horizontal Structure of 500 mb Height Fluctuations with Long, Intermediate and Short Time  
 309 Scales. *Journal of the Atmospheric Sciences*, 41(6), 961–980. Retrieved  
 310 2023-04-16, from [https://journals.ametsoc.org/view/journals/atsc/41/](https://journals.ametsoc.org/view/journals/atsc/41/6/1520-0469_1984_041_0961_hsomhf_2_0_co_2.xml)  
 311 6/1520-0469\_1984\_041\_0961\_hsomhf\_2\_0\_co\_2.xml (Publisher: American  
 312 Meteorological Society Section: Journal of the Atmospheric Sciences) doi:  
 313 10.1175/1520-0469(1984)041<0961:HSOMHF>2.0.CO;2
- 314 Blackmon, M. L., Wallace, J. M., Lau, N.-C., & Mullen, S. L. (1977, July). An  
 315 Observational Study of the Northern Hemisphere Wintertime Circulation.  
 316 *Journal of the Atmospheric Sciences*, 34(7), 1040–1053. Retrieved 2023-  
 317 03-31, from [https://journals.ametsoc.org/view/journals/atsc/34/](https://journals.ametsoc.org/view/journals/atsc/34/7/1520-0469_1977_034_1040_aosotn_2_0_co_2.xml)  
 318 7/1520-0469\_1977\_034\_1040\_aosotn\_2\_0\_co\_2.xml (Publisher: American  
 319 Meteorological Society Section: Journal of the Atmospheric Sciences) doi:  
 320 10.1175/1520-0469(1977)034<1040:AOSOTN>2.0.CO;2
- 321 Chen, G., Lu, J., Burrows, D. A., & Leung, L. R. (2015). Local finite-amplitude  
 322 wave activity as an objective diagnostic of midlatitude extreme weather.  
 323 *Geophysical Research Letters*, 42(24), 10,952–10,960. Retrieved 2023-03-24,  
 324 from <https://onlinelibrary.wiley.com/doi/abs/10.1002/2015GL066959>  
 325 (\_eprint: <https://onlinelibrary.wiley.com/doi/pdf/10.1002/2015GL066959>) doi:  
 326 10.1002/2015GL066959
- 327 Feldstein, S. B. (2000, December). The Timescale, Power Spectra, and Climate  
 328 Noise Properties of Teleconnection Patterns. *Journal of Climate*, 13(24),  
 329 4430–4440. Retrieved 2023-03-31, from [https://journals.ametsoc.org/](https://journals.ametsoc.org/view/journals/clim/13/24/1520-0442_2000_013_4430_ttpsac_2_0_co_2.xml)  
 330 view/journals/clim/13/24/1520-0442\_2000\_013\_4430\_ttpsac\_2\_0\_co\_2.xml  
 331 (Publisher: American Meteorological Society Section: Journal of Climate) doi:  
 332 10.1175/1520-0442(2000)013<4430:TTPSAC>2.0.CO;2
- 333 Green, J. S. A. (1977). The Weather During July 1976: Some Dynamical Consider-  
 334 ations of the Drought. *Weather*, 32(4), 120–126. Retrieved 2023-04-19, from  
 335 [https://onlinelibrary.wiley.com/doi/abs/10.1002/j.1477-8696.1977](https://onlinelibrary.wiley.com/doi/abs/10.1002/j.1477-8696.1977.tb04532.x)  
 336 .tb04532.x (\_eprint: [https://onlinelibrary.wiley.com/doi/pdf/10.1002/j.1477-](https://onlinelibrary.wiley.com/doi/pdf/10.1002/j.1477-8696.1977.tb04532.x)  
 337 8696.1977.tb04532.x) doi: 10.1002/j.1477-8696.1977.tb04532.x
- 338 Hartmann, D. L. (2015). *Global Physical Climatology: Second Edition* (2nd ed  
 339 ed.). Kent: Elsevier Science & Technology. Retrieved 2023-04-16, from  
 340 [https://public.ebookcentral.proquest.com/choice/publicfullrecord](https://public.ebookcentral.proquest.com/choice/publicfullrecord.aspx?p=5754480)  
 341 .aspx?p=5754480 (OCLC: 1099348114)
- 342 Hasselmann, K. (1976). Stochastic climate models Part I. Theory. *Tellus*,  
 343 28(6), 473–485. Retrieved 2023-04-19, from [https://onlinelibrary](https://onlinelibrary.wiley.com/doi/abs/10.1111/j.2153-3490.1976.tb00696.x)  
 344 .wiley.com/doi/abs/10.1111/j.2153-3490.1976.tb00696.x (\_eprint:  
 345 <https://onlinelibrary.wiley.com/doi/pdf/10.1111/j.2153-3490.1976.tb00696.x>)  
 346 doi: 10.1111/j.2153-3490.1976.tb00696.x
- 347 Held, I. M. (1999, January). The macroturbulence of the troposphere. *Tellus A: Dynamic Meteorology and Oceanography*, 51(1), 59–70. Retrieved 2023-04-19,  
 348 from <https://doi.org/10.3402/tellusa.v51i1.12306> (Publisher: Taylor  
 349 & Francis \_eprint: <https://doi.org/10.3402/tellusa.v51i1.12306>) doi: 10.3402/  
 350 tellusa.v51i1.12306
- 351 Huang, C. S. Y., & Nakamura, N. (2016, January). Local Finite-Amplitude Wave  
 352 Activity as a Diagnostic of Anomalous Weather Events. *Journal of the Atmospheric Sciences*, 73(1), 211–229. Retrieved 2023-03-24, from [https://](https://journals.ametsoc.org/view/journals/atsc/73/1/jas-d-15-0194.1.xml)  
 353 journals.ametsoc.org/view/journals/atsc/73/1/jas-d-15-0194.1.xml  
 354 (Publisher: American Meteorological Society Section: Journal of the Atmo-  
 355 spheric Sciences) doi: 10.1175/JAS-D-15-0194.1

- 359 Huang, C. S. Y., & Nakamura, N. (2017). Local wave activity budgets of the win-  
 360 tertime Northern Hemisphere: Implication for the Pacific and Atlantic storm  
 361 tracks. *Geophysical Research Letters*, *44*(11), 5673–5682. Retrieved 2023-03-31,  
 362 from <https://onlinelibrary.wiley.com/doi/abs/10.1002/2017GL073760>  
 363 (\_eprint: <https://onlinelibrary.wiley.com/doi/pdf/10.1002/2017GL073760>) doi:  
 364 10.1002/2017GL073760
- 365 Kidson, J. W. (1991, September). Intraseasonal Variations in the Southern Hemi-  
 366 sphere Circulation. *Journal of Climate*, *4*(9), 939–953. Retrieved 2023-  
 367 04-16, from [https://journals.ametsoc.org/view/journals/clim/4/  
 368 9/1520-0442\\_1991\\_004\\_0939\\_ivitsh\\_2\\_0\\_co\\_2.xml](https://journals.ametsoc.org/view/journals/clim/4/9/1520-0442_1991_004_0939_ivitsh_2_0_co_2.xml) (Publisher: Ameri-  
 369 can Meteorological Society Section: Journal of Climate) doi: 10.1175/  
 370 1520-0442(1991)004<0939:IVITSH>2.0.CO;2
- 371 Kushner, P. J., & Held, I. M. (1998). A test, using atmospheric data, of a  
 372 method for estimating oceanic eddy diffusivity. *Geophysical Research  
 373 Letters*, *25*(22), 4213–4216. Retrieved 2023-04-19, from [https://  
 374 onlinelibrary.wiley.com/doi/abs/10.1029/1998GL900142](https://onlinelibrary.wiley.com/doi/abs/10.1029/1998GL900142) (\_eprint:  
 375 <https://onlinelibrary.wiley.com/doi/pdf/10.1029/1998GL900142>) doi:  
 376 10.1029/1998GL900142
- 377 Leith, C. E. (1973, September). The Standard Error of Time-Average Estimates  
 378 of Climatic Means. *Journal of Applied Meteorology and Climatology*, *12*(6),  
 379 1066–1069. Retrieved 2023-04-19, from [https://journals.ametsoc.org/  
 380 view/journals/apme/12/6/1520-0450\\_1973\\_012\\_1066\\_tseota\\_2\\_0\\_co\\_2.xml](https://journals.ametsoc.org/view/journals/apme/12/6/1520-0450_1973_012_1066_tseota_2_0_co_2.xml)  
 381 (Publisher: American Meteorological Society Section: Journal of Applied  
 382 Meteorology and Climatology) doi: 10.1175/1520-0450(1973)012<1066:  
 383 TSEOTA>2.0.CO;2
- 384 Lorenz, D. J., & Hartmann, D. L. (2001, November). Eddy–Zonal Flow Feedback  
 385 in the Southern Hemisphere. *Journal of the Atmospheric Sciences*, *58*(21),  
 386 3312–3327. Retrieved 2023-03-31, from [https://journals.ametsoc.org/  
 387 view/journals/atsc/58/21/1520-0469\\_2001\\_058\\_3312\\_ezffit\\_2\\_0\\_co\\_2.xml](https://journals.ametsoc.org/view/journals/atsc/58/21/1520-0469_2001_058_3312_ezffit_2_0_co_2.xml)  
 388 (Publisher: American Meteorological Society Section: Journal of the Atmo-  
 389 spheric Sciences) doi: 10.1175/1520-0469(2001)058(3312:EZFFIT)2.0.CO;2
- 390 Nakamura, H., & Shimpou, A. (2004, May). Seasonal Variations in the South-  
 391 ern Hemisphere Storm Tracks and Jet Streams as Revealed in a Reanaly-  
 392 sis Dataset. *Journal of Climate*, *17*(9), 1828–1844. Retrieved 2023-04-  
 393 16, from [https://journals.ametsoc.org/view/journals/clim/17/9/  
 394 1520-0442\\_2004\\_017\\_1828\\_svitsh\\_2\\_0\\_co\\_2.xml](https://journals.ametsoc.org/view/journals/clim/17/9/1520-0442_2004_017_1828_svitsh_2_0_co_2.xml) (Publisher: Ameri-  
 395 can Meteorological Society Section: Journal of Climate) doi: 10.1175/  
 396 1520-0442(2004)017<1828:SVITSH>2.0.CO;2
- 397 Nakamura, N., & Zhu, D. (2010, September). Finite-Amplitude Wave Activity  
 398 and Diffusive Flux of Potential Vorticity in Eddy–Mean Flow Interaction.  
 399 *Journal of the Atmospheric Sciences*, *67*(9), 2701–2716. Retrieved 2023-  
 400 03-24, from [https://journals.ametsoc.org/view/journals/atsc/67/9/  
 401 2010jas3432.1.xml](https://journals.ametsoc.org/view/journals/atsc/67/9/2010jas3432.1.xml) (Publisher: American Meteorological Society Section:  
 402 Journal of the Atmospheric Sciences) doi: 10.1175/2010JAS3432.1
- 403 Swanson, K. L., & Pierrehumbert, R. T. (1997, June). Lower-Tropospheric Heat  
 404 Transport in the Pacific Storm Track. *Journal of the Atmospheric Sciences*,  
 405 *54*(11), 1533–1543. Retrieved 2023-04-19, from [https://journals.ametsoc  
 406 .org/view/journals/atsc/54/11/1520-0469\\_1997\\_054\\_1533\\_ltthtit\\_2\\_0  
 407 .co\\_2.xml](https://journals.ametsoc.org/view/journals/atsc/54/11/1520-0469_1997_054_1533_ltthtit_2_0_co_2.xml) (Publisher: American Meteorological Society Section: Jour-  
 408 nal of the Atmospheric Sciences) doi: 10.1175/1520-0469(1997)054<1533:  
 409 LTHTIT>2.0.CO;2
- 410 Thompson, D. W. J., & Barnes, E. A. (2014, February). Periodic Variability in  
 411 the Large-Scale Southern Hemisphere Atmospheric Circulation. *Science*,  
 412 *343*(6171), 641–645. Retrieved 2023-03-24, from [https://www.science.org/  
 413 doi/10.1126/science.1247660](https://www.science.org/doi/10.1126/science.1247660) (Publisher: American Association for the

- 414 Advancement of Science) doi: 10.1126/science.1247660
- 415 Thompson, D. W. J., Crow, B. R., & Barnes, E. A. (2017, March). Intraseasonal  
416 Periodicity in the Southern Hemisphere Circulation on Regional Spatial  
417 Scales. *Journal of the Atmospheric Sciences*, *74*(3), 865–877. Retrieved 2023-  
418 03-31, from [https://journals.ametsoc.org/view/journals/atsc/74/3/  
419 jas-d-16-0094.1.xml](https://journals.ametsoc.org/view/journals/atsc/74/3/jas-d-16-0094.1.xml) (Publisher: American Meteorological Society Section:  
420 Journal of the Atmospheric Sciences) doi: 10.1175/JAS-D-16-0094.1
- 421 Thompson, D. W. J., & Woodworth, J. D. (2014, April). Barotropic and Baro-  
422 clinic Annular Variability in the Southern Hemisphere. *Journal of the Atmo-  
423 spheric Sciences*, *71*(4), 1480–1493. Retrieved 2023-03-31, from [https://  
424 journals.ametsoc.org/view/journals/atsc/71/4/jas-d-13-0185.1.xml](https://journals.ametsoc.org/view/journals/atsc/71/4/jas-d-13-0185.1.xml)  
425 (Publisher: American Meteorological Society Section: Journal of the Atmo-  
426 spheric Sciences) doi: 10.1175/JAS-D-13-0185.1
- 427 Trenberth, K. E. (1981). Seasonal variations in global sea level pressure  
428 and the total mass of the atmosphere. *Journal of Geophysical Research:  
429 Oceans*, *86*(C6), 5238–5246. Retrieved 2023-04-16, from [https://  
430 onlinelibrary.wiley.com/doi/abs/10.1029/JC086iC06p05238](https://onlinelibrary.wiley.com/doi/abs/10.1029/JC086iC06p05238) (\_eprint:  
431 <https://onlinelibrary.wiley.com/doi/pdf/10.1029/JC086iC06p05238>) doi:  
432 10.1029/JC086iC06p05238
- 433 Trenberth, K. E. (1991, October). Storm Tracks in the Southern Hemisphere.  
434 *Journal of the Atmospheric Sciences*, *48*(19), 2159–2178. Retrieved 2023-  
435 04-16, from [https://journals.ametsoc.org/view/journals/atsc/48/  
436 19/1520-0469\\_1991\\_048\\_2159\\_stitsh\\_2\\_0\\_co\\_2.xml](https://journals.ametsoc.org/view/journals/atsc/48/19/1520-0469_1991_048_2159_stitsh_2_0_co_2.xml) (Publisher: American  
437 Meteorological Society Section: Journal of the Atmospheric Sciences) doi:  
438 10.1175/1520-0469(1991)048<2159:STITSH>2.0.CO;2
- 439 Vitart, F., Ardilouze, C., Bonet, A., Brookshaw, A., Chen, M., Codorean, C., ...  
440 Zhang, L. (2017, January). The Subseasonal to Seasonal (S2S) Prediction  
441 Project Database. *Bulletin of the American Meteorological Society*, *98*(1),  
442 163–173. Retrieved 2023-03-31, from [https://journals.ametsoc.org/view/  
443 journals/bams/98/1/bams-d-16-0017.1.xml](https://journals.ametsoc.org/view/journals/bams/98/1/bams-d-16-0017.1.xml) (Publisher: American Meteoro-  
444 logical Society Section: Bulletin of the American Meteorological Society) doi:  
445 10.1175/BAMS-D-16-0017.1
- 446 Wang, L., Lu, J., & Kuang, Z. (2018). A Robust Increase of the Intraseasonal Peri-  
447 odic Behavior of the Precipitation and Eddy Kinetic Energy in a Warming Cli-  
448 mate. *Geophysical Research Letters*, *45*(15), 7790–7799. Retrieved 2023-03-24,  
449 from <https://onlinelibrary.wiley.com/doi/abs/10.1029/2018GL078495>  
450 (\_eprint: <https://onlinelibrary.wiley.com/doi/pdf/10.1029/2018GL078495>) doi:  
451 10.1029/2018GL078495
- 452 Wang, L., & Nakamura, N. (2015). Covariation of finite-amplitude wave ac-  
453 tivity and the zonal mean flow in the midlatitude troposphere: 1. The-  
454 ory and application to the Southern Hemisphere summer. *Geophys-  
455 ical Research Letters*, *42*(19), 8192–8200. Retrieved 2023-04-16, from  
456 <https://onlinelibrary.wiley.com/doi/abs/10.1002/2015GL065830>  
457 (\_eprint: <https://onlinelibrary.wiley.com/doi/pdf/10.1002/2015GL065830>)  
458 doi: 10.1002/2015GL065830
- 459 Wang, L., & Nakamura, N. (2016, December). Covariation of Finite-Amplitude  
460 Wave Activity and the Zonal-Mean Flow in the Midlatitude Troposphere.  
461 Part II: Eddy Forcing Spectra and the Periodic Behavior in the Southern  
462 Hemisphere Summer. *Journal of the Atmospheric Sciences*, *73*(12), 4731–  
463 4752. Retrieved 2023-04-22, from [https://journals.ametsoc.org/view/  
464 journals/atsc/73/12/jas-d-16-0091.1.xml](https://journals.ametsoc.org/view/journals/atsc/73/12/jas-d-16-0091.1.xml) (Publisher: American Me-  
465 teorological Society Section: Journal of the Atmospheric Sciences) doi:  
466 10.1175/JAS-D-16-0091.1
- 467 Xue, D., Lu, J., Qian, Y., & Zhang, Y. (2021). Evidence for Coupling Be-  
468 tween the Subseasonal Oscillations in the Southern Hemisphere Midlat-

469 itude Ocean and Atmosphere. *Journal of Geophysical Research: Atmo-*  
470 *spheres*, 126(4), e2020JD033872. Retrieved 2023-03-31, from [https://](https://onlinelibrary.wiley.com/doi/abs/10.1029/2020JD033872)  
471 [onlinelibrary.wiley.com/doi/abs/10.1029/2020JD033872](https://onlinelibrary.wiley.com/doi/abs/10.1029/2020JD033872) (eprint:  
472 <https://onlinelibrary.wiley.com/doi/pdf/10.1029/2020JD033872>) doi:  
473 10.1029/2020JD033872